H_2SO_4 and particle production in a Photolytic Flow Reactor. Chemical modeling, cluster thermodynamics and contamination issues

David R. Hanson[1], Hussein Abdullahi[1], Seakh Menheer[1], Joaquin Vences[1], Michael R. Alves[1,2], and Joan Kunz[1]

[1] Chemistry Department, Augsburg University, Minneapolis, MN 55454, USA
[2] Chemistry and Biochemistry, University of California - San Diego, La Jolla, CA 92093, USA

Correspondence to: D. R. Hanson (hansondr@augsburg.edu)

Abstract. Size distributions of particles formed from sulfuric acid (H_2SO_4) and water vapor in a Photolytic Flow Reactor (PhoFR) were measured with a nano-particle mobility sizing system. Experiments with added ammonia and dimethylamine were also performed. $H_2SO_{4(g)}$ was synthesized from HONO, sulfur dioxide, and water vapor, initiating OH oxidation by HONO photolysis. Experiments were performed at 296 K over a range of sulfuric acid production levels and for 16 to 82 % relative humidity. Measured distributions generally had a large particle mode that was roughly log-normal; mean diameters ranged from 3 to 12 nm and widths ($\ln\sigma$) were ~0.3. Particle formation conditions were stable over many months. Addition of single-digit pmol/mol mixing ratios of dimethylamine led to very large increases in particle number density. Particles produced with ammonia, even at 2000 pmol/mol, showed that NH_3 is a much less effective nucleator than dimethylamine. A two-dimensional simulation of particle formation in PhoFR is also presented that starts with gas-phase photolytic production of H_2SO_4 followed by kinetic formation of molecular clusters and their decomposition determined by their thermodynamics. Comparisons with model predictions of the experimental results dependency on HONO and water vapor concentrations yield phenomenological cluster thermodynamics and help delineate the effects of potential contaminants. The added-base simulations and experimental results provide support for previously published dimethylamine-H_2SO_4 cluster thermodynamics and provide a phenomenological set of ammonia-sulfuric acid thermodynamics.

1 Introduction

Particle formation in the atmosphere has long been studied (McMurry et al. 2005; Kulmala et al. 2004) to ascertain potential impacts on health (Nel 2005) and on climate processes(IPCC 2013). For example, nano-particles (characterized as < 10 nm in diameter) can have special health effects as their small size allows for efficient transport into lung tissue (Kreyling et al. 2006). They also influence climate by growing to sizes large enough to affect radiative forcing and the properties of clouds. Despite numerous and wide-ranging studies devoted to understanding new particle formation, mechanisms and nucleation rates applicable to many regions of the atmosphere remain uncertain.

Sulfuric acid-driven nucleation is a prime source of nanoparticles in the atmosphere (Kuang et al. 2012; Sipilä et al. 2010) thus it is the starting point for many laboratory studies. Previous work on particle nucleation in the binary (water-sulfuric acid) system (Kirkby et al. 2011; Ball et al. 1999; Zollner et al. 2012; Ehrhart et al. 2016; Yu et al. 2017) have concluded that binary nucleation can be significant at low temperatures such as at high latitudes and in the upper troposphere. The sulfuric acid/water binary system also serves as an important baseline diagnostic for comparing experimental results. Finally, nanoparticle growth by sulfuric acid and water vapors is of interest as well as uptake of oxidized organic compounds by acidic nanoparticles. Good knowledge of the formation and stability of binary nano-particles is needed to understand their subsequent growth via other compounds.

Previous laboratory studies of nucleation in the binary system diverge widely, especially for results taken at or near room-temperature, suggesting experimental details may significantly affect results. For example, does it matter if H_2SO_4 is provided by a bulk or a photolytic source? Does the type of photolytic precursor- O_3, H_2O_2, H_2O, etc.-matter? (Sipilä et al. 2010; Berndt et al. 2008; Laaksonen et al. 2008) The CLOUD experimental results at 278 K and below (Kürten et al. 2016; Ehrhart et al. 2015) has alleviated some of these concerns yet room temperature results can provide more stringent tests due to a greater sensitivity to thermodynamics. Other issues include (i) limitations imposed by particle detector characteristics as well as cluster/particle wall losses (McMurry 1983; Kürten et al. 2015; 2018) and (ii) determining the concentration of H_2SO_4 (Sipilä et al. 2010; Kürten et al. 2012; Young et al. 2008) which is typically uncertain to a factor of two (Eisele and Tanner, 1993), although higher accuracies (±33%, Kürten et al. 2012) can be achieved. These experimental challenges can significantly influence results and their interpretation yet these largely known issues can be addressed to some degree.

Contaminants are the biggest unknown factor in these types of experiments and it is important to ascertain whether they are present at levels that can influence particle formation rates. If the contaminant is an amine, even a very low abundance can be a point of concern. For example, Zollner et al. (2012) argued that a 10^{-14} mixing ratio of methylamine could have affected their binary system measurements. Glasoe et al. (2015) presented data from the same apparatus as Zollner et al. and they carried this argument further and estimated that contaminant dimethylamine mixing ratios during their binary system measurements were less than or equal to 10^{-15}. If the contaminant is NH_3, however, it likely needs to reach the single-digit pmol/mol (pptv) level or higher to significantly interfere with measurements in the binary system at room temperature. Kirkby et al. (2011) and more recently Kürten et al. (2016) estimate ammonia contaminant levels of 4-to-10 pptv NH_3 for their experiments performed at 292 - 298 K; it is not clear if this level of ammonia had a significant effect on their results. Recently, Yu et al. (2017) reported upper limits for NH_3 and dimethylamine of 23 and 0.5 pptv, respectively, for their putative base-free nucleation experiments. Yet their nucleation rates are not extreme outliers, suggesting that their dimethylamine level was probably much lower than 0.5 pptv. Nonetheless, uncertainty introduced by undetectable (at the current state-of-the-art) levels of contaminants underscores the need for multiple approaches for studying sulfuric acid nucleation.

Here we describe an apparatus and results from experiments on the formation of sulfuric acid nanoparticles from photolytically-generated sulfuric acid vapor via $OH+SO_2$ photochemistry initiated with HONO photolysis at ~350-to-370

nm. Although nitrous acid is considered an important contributor to OH radical formation in many situations (Sörgel et al. 2011), little has been done to understand its photolysis that leads to sulfuric acid formation and new particle formation. We also studied the effects of adding ammonia or dimethylamine; both are known to greatly enhance particle production rates (Almeida et al. 2013; Glasoe et al. 2015; Yu et al. 2012; Ortega et al. 2012; Nadykto and Yu 2011). We present experimental results where temporary contamination of the apparatus was evident yet long-term results indicate a relatively constant level of cleanliness in the experiment. The experimental results are compared to simulations of the flow reactor that couple the flow with photo-chemical kinetics and an acid-base particle formation scheme. In addition to providing H_2SO_4 concentrations, the model results and their comparison to experimental particle characteristics has led to phenomenological cluster free energies for the ammonia-sulfuric acid system at 52 % relative humidity. Finally, we present a compendium of results from photolytic particle formation experiments near room temperature.

2 Methods

The Photolytic Flow Reactor (PhoFR) is a vertically-aligned cylindrical glass tube with an inner diameter of 5.0 cm, a length of ~130 cm, a volume of approximately 2.5 L and topped with a 23 cm long conical glass piece with several flow inlets (Fig. 1a). In the course of this work, a Teflon screen was positioned between the cone and the flow reactor to calm the jetting from the inlets. A ~ 105 cm length of PhoFR is jacketed and kept at a constant temperature, typically 296 K, by circulation of thermostated water. The main flow of gas was nitrogen from a liquid nitrogen gas-pack and the total flow rate was 2.9 sLpm (standard L / min, 273 K and 1 atm). The flow contained small amounts of SO_2 and HONO, typically 16 and 0.02 μmol/mol (ppmv), respectively, and up to several % water vapor; relative humidity was set by sending a portion of the flow over a heated water reservoir and then through a thermostated, vertically-aligned tube that removed excess water vapor. Total pressure was slightly above ambient, ~ 0.98 atm: gauge pressure was monitored continuously and it was typically 0.001 atm. The oxygen level from the liquid nitrogen, stated to be 10 ppmv or less, was apparently sufficient for the subsequent oxidation chemistry - noting little differences in particle size distributions upon adding several % O_2 to the flow. For all liquid nitrogen cylinder change-overs, the high pressure side of the regulator is flushed several times before exposing the lines to the new supply of gas - a standard procedure used by Ball et al., Zollner et al. and Glasoe et al. Also keeping in line with that past work, filters have not been used on any gas-supply lines.

Entering gas flows were monitored and set by mass flow meters under computer control. Typical flows for baseline conditions in sLpm or sccm (standard cm^3 / min, 273 K, 1 atm) were dry gas at 1.4 sLpm, fully humidified air at 1.5 sLpm, HONO-laden (~15 ppmv) N_2 flow at 4.2 sccm, and SO_2-laden flow at 32 sccm (1500 ppmv SO_2-in-N_2). These baseline conditions help diagnose the long term stability of the system. The baseline number densities of SO_2 and HONO in the flow reactor (accounting for dynamic dilution) are $4x10^{14}$ and $5.2x10^{11}$ cm^{-3}, respectively. Three sections were not insulated or thermo-regulated: (i) the conical top section, (ii) the top 10 cm of the flow reactor where the base-addition port resides, and

(iii) the bottom 20 cm where aerosol was sampled. The fully humidified line and the port where it enters the cone were gently heated (298-300 K) to eliminate condensation when room temperature was less than 296 K.

The SO_2-in N_2 mixture (Minneapolis Oxygen) was reported (Liquid Technologies Corporation, EPA Protocol) to contain 1500 ppmv SO_2 +/- 10%. Water vapor was taken from a gently heated ~500 mL volume of deionized water (Millipore) that also contained a few grams of concentrated sulfuric acid to suppress potential base contamination from the bulk water. This humidified flow then passed through 80 cm of vertically-aligned Teflon tubing (~6.2 mm ID) held at the temperature of the flow reactor.

Photolyte HONO was continuously produced (Febo et al. 1995) by flowing nitrogen laden with ~15 ppmv HCl vapor into a small (25 mL) round-bottom flask containing 1-2 grams of powdered NaONO(s), held at 40-50°C (Fig. 1b). HONO vapor and co-product NaCl(s) are produced in a classic double-displacement reaction. The powder could be very slowly mixed with a small (1 cm long) stir bar and results generally did not depend on whether the powder was stirred. Periodic gentle shaking of the flask usually led to only temporary changes in particle number densities.

The HONO level exiting the generator is likely to be equal to the HCl level entering it. The HCl-generator and a water vapor pre-saturator were temperature-controlled at typically 20 °C. A saturated (~6 m, molal) NaCl aqueous solution in the pre-saturator yields a relative humidity of 76 % in the flow: a stable amount of water vapor stabilizes the solution in the HCl-generator, which contains a solution with a 2-to-1 mole ratio for NaCl to H_2SO_4. The HCl-generator solution was prepared initially with concentrations of 3.5 m NaCl and 1.75 m H_2SO_4 and calculations (Wexler and Clegg, 2002; Friese and Ebel, 2010) result in an HCl vapor pressure of 9.3×10^{-6} atm. UV absorption measurements to determine the HONO level in this flow are described in the Supplement (S5.1) and results indicate that the source has a HONO level of about 1.5×10^{-5} atm. This suggests that the HCl-generator's HCl vapor pressure is slightly larger than the calculated value. While the water vapor pre-saturator minimized loss of water from the HCl-generator, small temperature differences between these two vessels can introduce variability and possibly a bias.

Four black lights that have a UVA spectral irradiance centered at 360 nm illuminated about a 115 cm length of the jacketed flow reactor from a distance of about 15 cm from the reactor center. An estimate of the fluence (5×10^{15} photon cm^{-2} s^{-1}) indicates a photolysis rate coefficient of approximately 10^{-3} s^{-1} for HONO. Described in the Supplement (S5.2) are experiments where production of methylvinylketone and methacrolein from the oxidation of isoprene were monitored, yielding (together with the 15 ppmv HONO level in the source flow) a HONO photolysis rate coefficient of 8×10^{-4} s^{-1}.

H_2SO_4 is formed via (i) OH produced via HONO photolysis, (ii) OH addition to SO_2, (iii) H-atom abstraction by O_2 and (iv) reaction of SO_3 with H_2O molecules (Lovejoy et al., 1996). The HO_2 and NO radicals generated in this process can react together and generate an additional OH radical. When SO_2 is present at a few ppmv, the dominant loss for OH is OH + SO_2: a pseudo-first-order loss rate coefficient is given by $[SO_2]^* k_{OH+SO2} = 4 \times 10^{14}$ cm^{-3} * 8.9×10^{-13} $cm^3 s^{-1} = 360$ s^{-1}. With this SO_2 baseline level, OH reacts with HONO for typical conditions only about 1 % of the time: the OH first-order loss rate coefficient is ~3 s^{-1}, from $[HONO]^* k_{OH+HONO} = 5 \times 10^{11}$ cm^{-3} * 6×10^{-12} $cm^3 s^{-1}$. Yet at low SO_2 levels, loss of OH due to reaction with HONO can be significant.

H_2SO_4 levels build as the flow moves down the reactor, forming H_2SO_4 molecular clusters and these clusters grow into stable particles. These particles accumulate enough material, primarily H_2SO_4 and H_2O, to grow to several nm in diameter. Growth due to OH or HO_2 uptake followed by reaction with absorbed SO_2 may also contribute to growth.

Particles were sampled on axis at the exit of the flow reactor, about 120 cm from the conical inlet, with a custom-built mobility-sizing and counter system designed for nanometer-sized particles. Briefly, size-classified particles (Am-241 charger and a TSI 3085 nanoDMA) were detected with a diethyleneglycol (DEG), sheathed condensation particle counter (CPC) in tandem with a butanol-based CPC (Jiang et al. 2011). This system is denoted 'DEG system' in this study. The DEG CPC was operated with a saturator temperature of 57°C, a condenser temperature of 20°C, 0.36 L/min condenser flow and 0.07 L/min capillary flow. The nanoDMA was operated with 2 L/min aerosol-in and monodispersed-out flows and a 13 L/min sheath flow, as in Glasoe et al. (2015).

For a few experiments, ammonia or dimethylamine as trace gases were added through a port at the top of the flow reactor. A discussion of their mixing into the main flow is presented in the Supplement (S7.1). Their sources were permeation tubes, and 100s or single-digit pptv levels could be set by either a single- or a double-stage, respectively, dynamic dilution system (Freshour et al. 2014; Glasoe et al. 2015). Ammonia was used in the single-dilution system and dimethylamine was dedicated for use in the double-dilution system. Permeation rates were determined periodically by re-directing the base-laden flow through an acidic solution and monitoring the change in pH over time (Freshour et al., 2014).

2.1 Model

The 2-dimensional model of the flow reactor incorporating the photochemical kinetics of H_2SO_4 formation was built on a previous model of acid-base molecular cluster formation which was fully corroborated against a commercial computational fluid dynamics simulation (Hanson et al. 2017). The flow profile can be set to either plug or fully-developed laminar, the formation of clusters with up to ten H_2SO_4 and ten base molecules can be simulated. If so desired, clusters larger than ten H_2SO_4 molecules can be simulated using a growth-only mechanism. Note that clusters without a base molecule represent a weighted average of the binary H_2SO_4-H_2O thermodynamics for a given relative humidity. The detailed photochemistry in our experiment includes the production of OH, its reactions with SO_2 as well as with HO_2, NO, NO_2, HONO, HNO_3, H_2O_2 etc. The rate coefficients and mechanisms are presented in the Supplement (S7, Table S1). The acid and base species and all molecular clusters as well as OH are lost to the walls limited only by diffusion.

The model reacts, convects and diffuses all reactants and products and yields the abundance of H_2SO_4 and its molecular clusters, the largest clusters are then correlated to the abundance of experimentally determined particles (Panta et al. 2012; Hanson et al. 2017). Coagulation was not implemented, because cluster-cluster interactions are not significant for most of the conditions of the present work. Water molecules are not explicitly tracked but hydration is taken into when calculating the collisional rate coefficient and the size of the clusters, assuming bulk properties. Increases in computational times can be significant when large clusters are simulated using the growth-only mode, e.g. a factor of eight for adding clusters up to 250 H_2SO_4 molecules compared to stopping growth at the 10 acid, 3 base cluster. Yet it is desirable to simulate very large

clusters via uptake of H_2SO_4 assuming no loss to compare results to measured size distributions. Further analysis of cluster growth and loss processes, including growth-only for clusters larger than 10 H_2SO_4 molecules, is presented in the Supplement (S1.3).

Ammonia or dimethyl amine could be included at a trace level with the flow entering the simulated reactor whereupon acid-base clustering and particle formation commence (note that base is lost to the wall, limited by diffusion). The model assumes rapid mixing of base into the main flow. Justification for this is presented in the Supplement (S7.1). The photochemistry is described in detail in the Supplement (S7) and the acid-base clustering reactions are described in detail in Hanson et al. (2017) along with thermodynamic schemes for clusters of the bases with sulfuric acid. Scheme DMA_I from that work was used here while a new cluster thermodynamics scheme for the ammonia-added experiments was developed for NH_3-H_2SO_4 clusters at 52 % relative humidity (see S8).

3 Results and Discussion

3.1 Particle formation evaluation.

The stability of particle formation conditions over several months is demonstrated by presenting the number and the average size of particles for baseline conditions. In the next section, the modeled photochemistry for baseline conditions is presented to provide baseline sulfuric acid concentrations within PhoFR and we discuss how the size distributions were analyzed. In subsequent sections, these analytical devices will be applied to the results of experiments where reactant levels were varied. In the Supplement (S1.0) is a typical time series of the raw data (the count rates for each channel) and a table with the overall correction factors.

Shown in Figure 2 are (a) the total particle number density, N_p, and (b) so-called "leading-edge" (see S1.1 in the Supplement) mode diameters over a 6 month period for baseline conditions: 52 % relative humidity (RH), 296 K, total flow of 2.9 sLpm, and a flow of N_2 through the HONO source, Q_4, of 4.2 sccm. The data were binned according to the flow of the SO_2 mixture, Q_1, either 4 sccm or > 16 sccm. The abundance of HONO is 20 ppbv and SO_2 is either 2 ppmv or > 8 ppmv. Shown in the Supplement (S1.2) are representative particle size distributions - corrected for size-dependent diffusion losses in CPC transport and inlet lines. N_p was determined by summing the particle concentrations with D_p of ~2.4 nm and larger because the two smallest diameter concentrations are the local minimum for most of the size distributions. Furthermore, these small diameter data can have large random uncertainties due to large corrections applied to low count rates. Discussed in the Supplement (S4) are possible sources of the scatter in the data.

Note the data presented as gold diamonds: these are N_p (low SO_2) on the day of, and the day after, a gas supply cylinder change-over. This event could be due to entrainment of dust particles into the supply lines. Nothing like this happened on the five other cylinder change-overs that occurred during this time interval. What is different about this cylinder exchange is not known. The effects are temporary as a 90 % decrease in N_p occurred in a few hours, an additional 70 % drop occurred overnight and a day later N_p is within the upper range of the scatter for baseline conditions.

The measured size distributions are governed by the interplay between the spatial distribution of [H_2SO_4], whether base is added, and the nature of potential contaminant species. For example, small- and mid-sized particles probably form somewhat downstream of the top of the reactor whereas the largest particles at the leading edge of the distributions are formed near the top of the reactor. The largest particles must originate at the top of the reactor, having the highest overall exposure to H_2SO_4. These so-called leading-edge particles are the focus of our analysis.

The leading-edge particles are greatly enhanced when base was added, whether ammonia or dimethylamine. In these cases, the leading-edge particles are prominent in the distributions and are described by log-normals (see the distributions presented below). The leading-edge volume-mean diameters for the added-base experiments are similar to those of the no-added base distributions. So we propose that the leading-edge particles are indicative of the nucleation conditions at the top of PhoFR. In the Supplement (S1.1) is more discussion of the leading-edge mode of the particle size distributions and supporting results from the simulation (S1.2: plots of modeled distributions with and without added NH_3.)

The high SO_2 data (Fig. 2a) exhibits an N_p that averages about $2x10^4$ cm^{-3} since late February; also the leading edge of the size distributions (Fig. 2b), fit to log-normal functions, indicate mode diameters of about 6 nm with $\ln\sigma$ values of ~0.35. The large drop in N_p on the 23rd of February is due to a Teflon mesh (ultrasonically cleaned and soaked overnight in a dilute sulfuric acid solution) placed between the cone and the flow reactor. The edges of the Teflon mesh fit in the gap of the glass joint without disturbing the Teflon-encapsulated o-ring. The mesh was installed because flow visualization experiments, similar to those described in Ball et al. (1999), revealed extensive back-streaming into the cone. Back-streaming can carry H_2SO_4 from the illuminated section into the cone to initiate nucleation there. With the Teflon mesh in place, a trend in N_p with time cannot be discerned in Fig. 2a. Similarly, leading-edge mode diameters indicate that D_{le} is roughly constant over the time period Feb 24 to Jun 20 (Fig. 2b).

While the effects on N_p (Fig. 2a) due to the addition of the mesh are large, the effects on mode diameter are less pronounced. On the other hand, there is a five week period beginning the middle of April 2018 that has mode diameters about 1 nm larger than those during the preceding and following time periods. What was different about this time period is not known however potential changes in flow patterns and variations in room temperature are potential explanations.

Since changes in D_{le} are small or negligible, the growth conditions in PhoFR must be stable during this 5-month time period. The cumulative exposure of particles to H_2SO_4 as they travel down PhoFR is constant, indicating that the UV flux and reactant concentrations are also. The overall stability in N_p during this time also indicates that the purity of the system is stable. Variations in N_p might have been influenced by changes in potential contaminants, yet the HCl source for the HONO generator is temperature-sensitive and flow patterns can be influenced by temperature variations of the non-thermoregulated sections of the flow reactor. An expected increase in cleanliness over time, due to acid building up on surfaces and binding potential base-emitting contaminants, is not exhibited in the data.

3.1.1 Simulated reactant distributions

Shown in Fig. 3 are simulated centerline concentrations of the gas-phase species and two molecular clusters. In order of abundance at the end of the reactor on the left axis: H_2SO_4, NO_2, NO, HO_2, H_2O_2, HO_2NO_2 and NH_3; and on the right axis, OH, $(H_2SO_4)_2$ and 10^3 times the $(H_2SO_4)_{10}$ cluster abundance. This simulation was performed with [HONO] = 5.2×10^{11} cm^{-3}, simulating an experiment with Q_4 = 4.2 sccm. These conditions are close to those for the data depicted in Fig. 2 with the simulation being strictly binary nucleation.

Sulfuric acid rises steadily and reaches 1.2×10^{10} cm^{-3} by the end of the lighted section that extends from 0 to 110 cm. The downstream section of the reactor with the highest sulfuric acid level is where particles achieve most of their growth: over the bottom 2/3 of PhoFR, an axial distance of 40 to 125 cm, [H_2SO_4] averages about 8×10^9 cm^{-3}. We partition the reactor into a top third and a bottom two thirds. Although somewhat arbitrary, it provides a point of view for discussing the experimental results. Furthermore, this point of view is congruent with the experimental finding that a large particle mode at the leading edge of the size distributions is discernible, especially so when base was added. So although clusters are formed and particles are nucleated along the length of the reactor, we seek to explain only the largest of them.

With this perspective, we can calculate from bulk properties the growth of the leading-edge particles due to their accumulating H_2SO_4 and H_2O (assuming no evaporation) as they traverse the bottom 2/3 of the flow reactor. Using centerline values, an increase in particle diameter of 4.8 nm is estimated as they travel from 40 to 125 cm, using the bulk approximation to calculate the increase in diameter (Verheggen and Mozurkewich, 2002; Wexler and Clegg, 2002). This is in accord with the leading-edge mode diameters in Fig. 2b of about 6 nm, considering that nascent particles are roughly 1.3 nm in diameter; using bulk properties for the 4 acid cluster assuming it is large enough for evaporation to be negligible. There is also a 0.3 nm difference between mobility and volume/mass diameters (Larriba et al. 2010). Thus modeled H_2SO_4 on-axis concentrations and residence time along with the assumption of bulk properties for the small particles is an adequate starting point for discussing growth in this experiment.

Growth was also explored with the model and simulated particle size distributions (Supplement, S1.3. Fig. S7.1) are consistent with the growth calculation in the preceding paragraph. The simulated clusters were grown to hundreds of H_2SO_4 molecules using growth-only for clusters larger than 10 H_2SO_4 molecules. The ammonia-added simulations show a D_{le} of about 4 nm (Fig. S1.3.1b) and 6 nm (Fig. S7.1) for Q_4 = 2.1 and 4.2 sccm, respectively. These mode diameters are consistent with the bulk-properties growth analysis.

The added-base simulations also provide information on nucleation near the top of the reactor. The axial distribution of critical clusters, assumed to contain 4 H_2SO_4 molecules, and those just larger reach a steady state by about 40 cm (Fig. S1.3.2) while very few of the 20 and larger H_2SO_4 clusters have yet formed. Nucleation in the top third of the flow reactor is important and heavily influences the large particle mode when base is present. Downstream regions contribute mid-sized particles that influence the shape of the simulated particle size distributions; this can be seen in binary, added-dimethylamine and added-ammonia simulations that are compared in Figs. S1.3.1c. Nonetheless, these simulations support a partitioning of

the reactor as a rhetorical tool for discussing the results and for drawing broad conclusions about the presence of contaminants in this region.

3.2 Variation of N_p with [reactant]

3.2.1 Dependence on HONO

Shown in Fig. 4a are N_p vs. Q_4, the flow through the HONO source while the other reactants were held constant: 296 K, 52 % RH, SO_2 at 8 ppmv or higher. The data are primarily measurements without added base (black squares) but the results from two runs where base was added are also shown. Fig. 4b are typical size distributions for measurements at Q_4 = 4.2 sccm for experiments with and without added base. Several more representative size distributions as a function of Q_4 are shown in the Supplement (S1.2).

The N_2 flow through the HONO source, Q_4, is a proxy for HONO abundance and thus sulfuric acid. The variation of the volume-mean diameter of the leading-edge mode with Q_4 is presented in the Supplement (Fig. S1.2.2) and particle size scales approximately linearly with Q_4. This suggests that particles are exposed to linearly increasing amounts of H_2SO_4 over this range of Q_4. This data supports the Q_4-as-proxy notion that H_2SO_4 levels are proportional to the HONO concentration in PhoFR which is set by the nitrogen flow (Q_4) through the HONO source.

The nominally binary N_p has a power-dependence on Q_4 of about 4 (dashed line) which is also the case for the NH_3 added (230 pptv) data. For ammonia added at this level there is only a modest effect on N_p, a qualitative finding that is not congruent with recent experimental work (Kürten et al. 2016; Glasoe et al. 2015). For added dimethylamine at ~ 2 pptv, however, there is a large effect on N_p and on its dependence on Q_4, consistent with other experimental work (e.g. Glasoe et al.; Almeida et al. 2013). More results and discussion of the added-base experiments are presented below.

A power dependence of 5 for N_p on H_2SO_4 was exhibited for the H_2SO_4-H_2O binary system (Zollner et al. 2012) which is somewhat larger than that exhibited in Fig. 4b; other bulk experiments have power dependencies on H_2SO_4 that range up to ~20 (Wyslouzil et al. 1991; Viisanen et al. 1997). Yet the CLOUD experiment (Kürten et al. 2016), also with photolytic generation of H_2SO_4, shows a power dependency of 3.7 at 292 K for [H_2SO_4] concentrations from $3x10^8$ to $1.5x10^9$ cm^{-3}. An ammonia-contaminant abundance of 4 pptv was stated to apply to those results. Experimental results (Glasoe et al. 2015; Almeida et al. 2013) indicate power dependencies on H_2SO_4 are significantly affected when a base is present, corraborating the assertion that our nominally pure results were affected by the presence of an impurity base compound.

3.2.2 Effects of added ammonia and dimethylamine.

When base was added to PhoFR, its mixing ratio was calculated assuming it has fully mixed and there is no loss to the wall. There is wall loss in the experiment and mixing of the base into the main flow takes an amount of time. Nonetheless, these mixing ratios are convenient for discussion and they are directly linked to the flow of added base. Care needs to be

taken using these mixing ratios when comparing the results with simulations and other experiments. See the Supplement (S3.1 and S7.1) for more on base mixing into the flow.

With data for nominally clean conditions for comparison, the effect of 230 pptv NH_3 on the large particle abundance is significant in Fig. 4a, about a factor of 5, a factor that does not significantly depend on the level of HONO and thus H_2SO_4 present in the flow reactor. The experimental size distributions (e.g. red triangles in Fig. 4b) reveal a more distinct and larger leading edge mode than the nominally pure data. Plots of D_{le} as HONO was varied are presented in the Supplement (S3.1) and the effect of added NH_3 is a ~20% increase in D_{le}. The shift in the distributions to slightly larger sizes is due to enhanced particle formation in the top third of the flow reactor, shifting upstream the peak nucleation rates compared to that in the absence of added NH_3. This is supported by the simulated size distributions shown in the Supplement (S1.3) where the leading-edge of the size distributions becomes more distinct when ammonia is added to the simulations (Figs. S1.3.1).

Previous work has shown large increases in N_p when ammonia was added to a (nominally clean) binary sulfuric acid-water nucleating system. At H_2SO_4 concentrations of a few times 10^9 cm^{-3}, Ball et al. (1999), Zollner et al. (2012), and Glasoe et al. (2015) observed factors of 10-to-1000, ~1000, and 10^6 for ammonia levels of a few pptv, 25 pptv, and 55 pptv, respectively. Also, Kürten et al. (2016) showed that particle production in the CLOUD experiment increased by about a factor of 100 upon addition of several hundred pptv NH_3 at 292 K and $[H_2SO_4]$ of 1.5-2.2x10^8 cm^{-3}: this factor may have been even larger if the nominally binary system was not affected by a purported 4 pptv ammonia contaminant. We think that the presence of a contaminant in our nominally pure measurements is responsible for the low enhancement factors in particle numbers when 100s of pptv NH_3 are added. There will be more discussion on this below.

Dimethylamine addition at 2 pptv (+100/-50%) had a large effect on the number of particles (blue circles, Fig. 4a) and even the smallest particles (mobility diameter of 1.7 nm) increased by about 2 orders of magnitude (Fig. 4b). Nonetheless, the leading edge of the distributions is clearly the dominant mode for these conditions. It is interesting that the shape of the distributions is similar to the nominally binary cases (black diamonds, Fig. 4b). The Supplement (S3.2) presents additional measured size distributions for the dimethylamine-added experiments.

It is notable that N_p is not particularly sensitive to H_2SO_4 above Q_4 = 2.7 sccm. Model results also indicate a leveling off in the calculated N_p as Q_4 increases (see section 3.3 below) which appears to be due to scavenging of the amine by particles. Nonetheless, it appears that the potential contaminant for the nominally binary experiments is a much less effective nucleator than dimethylamine is at a level of 2 pptv.

Since effects due to adding dimethylamine at the single-digit pptv level are large, it would be desirable to experimentally investigate amine additions at lower levels. With the current dynamic dilution system, base addition at levels lower than a few pptv are swamped by the precision uncertainty in the flow meter readings. More results from these types of experiments await further improvement in the dimethylamine delivery system. Another alternative is exploring conditions where nucleation is expected to slow such as at low Q_4 and/or at temperatures warmer than 296 K.

3.2.2.1 Variation of N_p with added base.

Shown in Fig. 5 are the total number of particles plotted as a function of added ammonia level for a fixed amount of HONO either Q_4 = 2.1 (yellow) or 4.2 (red) sccm. The open squares represent the range of data obtained for nominally binary conditions (without added base). There are significant effects on N_p due to the addition of NH_3 at the top of the reactor, over a factor of ten for both sets of data.

At large NH_3 exposures (high levels and/or prolonged addition) particle counts increased dramatically with exposure time, indicating a conditioning of the flow reactor wall. This is demonstrated in the Supplement (S6) that presents measurements on days when 2000 pptv NH_3 was added. The 2000 pptv NH_3 data in Fig. 5 were taken soon after ammonia introduction, minimizing the effects of high ammonia exposure.

The large variability of the NH_3 data in Fig. 5 mirrors the underlying variability in N_p without added NH_3 (Fig. 4a). Yet, within the scatter of the measurements the dependence of N_p upon NH_3 is smaller than the 1.6 power dependence found in the bulk-source experiments of Glasoe et al. (2015). A close to linear dependence on ammonia can be ascertained from the results of other photolytic H_2SO_4 production experiments: the flow reactor experiments of Benson et al. (2009, 2011) and Berndt et al. (2010), and the 292 K CLOUD chamber experimental results (Kürten et al. 2016; Kirkby et al. 2011). On the other hand, the 292 K ACDC theoretical ammonia-sulfuric acid nucleation rates predict a power dependence on ammonia of between 2 and 3, depending on conditions (Kürten et al. 2016).

Simulated N_p as a function of added ammonia is shown in Fig. 5 and they are roughly in accord with the experimental data. The major discrepancy is at low added NH_3 where simulated N_p is significantly lower than experimental N_p. The presence of a contaminant that influences the experimental N_p, particularly at low ammonia levels, can contribute to this discrepancy. At high NH_3 levels, the effect of the contaminant was assumed to be diminished and the cluster thermodynamics were adjusted so that simulations matched experiment. Thus the experimental data at Q_4 = 4.2 sccm with ammonia $\geq$ 500 pptv guided the development of the H_2SO_4-NH_3 cluster thermodynamics used in these simulations (see the Supplement S8). We do not seek to establish the accuracy of the cluster thermodynamics but instead a phenomenological description of the results: the NH_3-H_2SO_4 thermodynamics developed and used here are phenomenological.

Incomplete agreement across the full range of the present experimental results can also be due in part to an inadequate representation of the actual flow and the mixing of base into the flow in the simulations, however, this would not be expected to depend on the amount of added-ammonia or on Q_4 (see Supplement S7.1 for more on base mixing into the flow.) Small changes to a few cluster free energies, 1 or 2 kcal/mol, can significantly alter predicted N_p.

For ammonia levels greater than a few hundred pptv, this set of thermodynamics (labeled NH3_52) yields simulated N_p that varies with NH_3 to the 1.6 power for Q_4= 4.2 sccm conditions and NH_3 to the 1.9 power for the Q_4=2.1 sccm conditions. Since the dependencies on NH_3 for these simulations and those of the theoretical ACDC rates (Kürten et al. 2016) are greater than is exhibited in the present and previous work (Benson et al. 2011; Berndt et al., 2010; Kürten et al. 2016; Kirkby et al. 2011), there may be a commonality across this set of experimental work: that contaminants affected the nominally binary

measurements. The low dependence of particle formation rate on ammonia (or low 'enhancement factors' e.g. Benson et al., 2011) exhibited in previous work (Benson et al. 2011; Berndt et al. 2010; Kirkby et al. 2011; Kürten et al. 2016) may have been due in part to the influence of contaminants. A 'saturation effect' at high ammonia levels may also act to limit (Kirkby et al. 2011) the ammonia dependence of the nucleation rate. Yet there is congruence of results from a few of the experiments at high ammonia conditions (see 3.4.1 below.)

The added-dimethylamine data in Fig. 5 show that dimethylamine has a very large effect on N_p, 2 to 3 orders of magnitude (Q_4 = 2.1 sccm for this data). There is a low dependency on dimethylamine abundance where N_p scales approximately linearly with amine mixing ratio. Simulations using DMA_I thermodynamics (Hanson et al. 2017) are also shown in Fig. 5 and simulated N_p mimic fairly well the experimental N_p and its variation with dimethylamine, except perhaps at 30 pptv dimethylamine where simulated N_p is $3x10^7$ cm^{-3}. Coagulation would reduce simulated N_p considerably: with a coagulation rate coefficient of $2x10^{-9}$ cm^3/s, an N_p of $3x10^7$ cm^{-3} results in a coagulation rate of $2x10^{-9}(3x10^7)^2$ = $2x10^6$ cm^{-3} s^{-1}. In just five seconds, a third of the simulated particles can coagulate. This rough estimate suggests coagulation is important for those conditions and the effect should be properly evaluated in the simulations.

The dimethylamine results presented in Figs. 4 and 5 are small sets of data and for Fig. 4 dimethylamine was added at a level that challenges the lower range of the dynamic dilution system. Nonetheless, the thermodynamic scheme DMA_I yields cluster concentrations that are consistent with the measured N_p and its trends with dimethylamine level. Since the thermodynamics scheme DMA_I (Hanson et al. 2017) was developed by comparing to the dimethylamine-H_2SO_4 data of Glasoe et al. (2015), the present data and the Glasoe et al. dimethylamine results are tied together in a semi-quantitative sense.

3.2.3 Water variation and addition of dimethyl amine..

Shown in Fig. 6 as filled squares are measured N_p vs. humidity, calculated from the flow rate of the humidified nitrogen. Total flow rate, HONO, and SO_2 levels were kept constant; the humidified flow rate was varied from 0.5 to 2.4 sLpm. Although the overall data is phenomenologically exponential (the solid line in the figure), over limited ranges the data exhibits power dependencies on RH of between 4 and 6. A strong dependence of the number of particles on RH is expected for the binary sulfuric acid water nucleating system, and the power dependence here lies at the low end of range (5-to-9) reported by Zollner et al. (2012). A plot of the size of the leading edge mode vs. humidity is presented in the Supplement (Fig. S1.2.2b).

A set of data with 2-to-5 pptv dimethylamine added is shown as the diamonds (filled and open are Q_4=4.2 and 2.1 sccm, respectively). There is much less water dependence (approximately linear) when dimethylamine is present which is consistent with theoretical notions (Almeida et al. 2013; Henschel et al. 2016) that dimethylamine-H_2SO_4 clusters are not particularly sensitive to H_2O. This postulate has also been elucidated in several other publications (e.g. Kurten et al. 2008; Coffman and Hegg, 1995). The data indicates there may be a slightly higher sensitivity to water vapor at the low Q_4 conditions. A complicating factor in fully interpreting this data is that the steady-state H_2SO_4 abundance (the monomer and

all its hydrates) changes with RH because its overall diffusivity changes about 10 % as RH varies from 15 to 80 % (Hanson and Eisele, 2000.) More experimental work is needed in this interesting system.

Supposing there are dimethylamine-type base contaminants in the putatively base-free experiments (solid squares), it clearly does not reach the single digit pptv level for baseline 52 % RH conditions. Indeed, simulated particle number densities with a level of 0.005 pptv dimethylamine entering the flow reactor were consistent with the 52% RH, Q_4=4.2 sccm results (see section 3.3 below). A set of simulations were run from 0.005 up to 2 pptv dimethylamine and predicted N_p scaled linearly with base level. At the 2 pptv level, an N_p of about 10^7 cm^{-3} was predicted while experimental N_p is $3x10^6$ cm^{-3}. Note that an N_p at the 10^7 cm^{-3} level will be significantly affected by coagulation which is not captured in the simulations.

3.2.4 SO_2.

Particle size and number density were found to depend on SO_2 abundance. Shown in Fig. 7 is N_p vs. the flow rate of the SO_2 mixture, Q_1. HONO source flow rate Q_4 was 4.2 sccm for this data. Despite its scatter, the data show the SO_2 level affects both the number of large particles and their size, $D_{V,le}$ (shown in Fig. S1.2.2c): both increase with [SO_2] and begin to level-off at high [SO_2]. This qualitative behavior is expected as at low SO_2 abundance not all of the OH will react with SO_2 and above a certain level there should not be much more of an effect with increases in SO_2. Young et al. (2008) also report a stronger-than-expected dependence of their results on SO_2 abundance.

A set of simulations that includes a reaction between HO_2 and SO_2 is shown as the solid line in Fig. 7. Note that a level of 200 pptv of NH_3 entering the flow reactor was included. The experimental results show increases with SO_2 that are roughly in line with the model simulations. Without this reaction the model shows (the dashed line) much smaller increases in N_p (40 % vs. 250 % with the reaction) and in size (Fig. S1.2.2c, 10% vs. 20% with the reaction) as SO_2 increases from 2 to 16 pptv.

The simulation assumed a value of $3x10^{-17}$ cm^3/s for $k_{HO2+SO2}$. There is disagreement whether HO_2 reacts with SO_2 as well as potential end products (Chen et al. 2014; Kurten et al. 2011); we assumed H_2SO_4 and OH. Experimental values for this rate coefficient range from upper limits of $1x10^{-18}$ cm^3/s (Graham et al. 1979) and $2x10^{-17}$ cm^3/s (Burrows et al. 1979), to a value of $8x10^{-16}$ cm^3/s (Payne et al. 1973). A heterogeneous reaction occurring in the particles involving SO_2 would help explain the dependence of $D_{V,le}$ on SO_2 abundance (Fig. S1.2.2c) while leaving N_p undisturbed.

3.3 Characteristics of a potential contaminant

Shown in Fig. 8 are the experimental N_p as a function of HONO from Fig. 4a along with model simulated N_p. The simulations were run for NH_3 at 0 and 200 pptv using NH3_52 thermodynamics and for dimethylamine at 0.005 pptv using DMA_I thermodynamics (Hanson et al. 2017). The experimental data is for nominally-clean conditions.

The simulations with NH_3 at 200 pptv yield N_p similar to the experimental and furthermore dependencies upon HONO align with experimental dependencies. The powerful nucleator dimethylamine entering the flow reactor at 5 ppqv (1.2 $x10^5$

cm^{-3}) also yields a simulated N_p at Q_4 = 4.2 sccm close to the experimental N_p of about $2.5x10^4$ cm^{-3}. The variation of predicted N_p with HONO, however, is disparate from the experimental variation, where the simulated N_p levels off at high values of Q_4. This leveling off is due, at least in part, to a simple number limitation: the largest simulated N_p is $4x10^4$ cm^{-3} which is about one third of the number density of dimethylamine molecules introduced. A strict limit would be reached depending on how many dimethylamine molecules are in each particle. Nonetheless, the simulations suggest the contaminant acts more like ammonia than dimethylamine.

While the presence of 200 pptv ammonia is consistent with the experimental N_p, methylamine has comparable power dependencies on acid. These are plotted as the purple circles in Fig. 8 where the methylamine nucleation rates were taken from the expression in Table S2 of Glasoe et al. (2015) and a 4 s nucleation time was applied. Since it is significantly less powerful than dimethylamine, a larger abundance of 0.5 pptv is needed to give N_p comparable to the experiment and the full range of Q_4 is covered, assuming scavenging of methylamine by clusters would be minimal. An impurity with an abundance of a fraction of a pptv may last a long time due to a low evaporation rate. These considerations would make methylamine (or perhaps another primary amine) a suitable candidate for a potential gas-phase base contaminant in PhoFR. Of course, whether the contaminant is ammonia or methylamine (or perhaps a combination) cannot be determined at this time. However, it appears that studying the primary amines would be interesting in this context as well as for understanding their effects on sulfuric acid nucleation rates. The Supplement (S9) presents some more discussion on the effects of SO_2.

3.4 Comparison to previous results.

A number of previous results are compiled along with the present measurements in Fig. 9 for nominally base-free conditions. The present results are assigned the simulated H_2SO_4 value in the center of the reactor and at 30 cm into the illuminated region. The nucleation rate J was taken to be N_p divided by the time the center of the flow travels from 20 to 40 cm, 4 s. This time is presumed to apply for the nominally clean conditions here. On the other hand, with base added intentionally, significant nucleation may also occur in the 0 to 20 cm region where base abundance is high. Uncertainties in J are probably on the order of a factor of 2. Uncertainty in H_2SO_4 is about a factor of two, based on the calculated values at 15 and 60 cm, which are -49 and +106 %, resp., from the 30 cm value. The radial profile of H_2SO_4 at 30 cm axial distance is flat from the center out to a radius of 1.7 cm. See the Supplement for radial profiles of H_2SO_4 (Fig. S1.3.3).

The experimental data in Fig. 9 were taken over a range of temperatures, 288 to 300 K, and relative humidities, 2.3 to 75 % RH; conditions indicated in the legend. The present results extrapolate to rates that are in fair agreement with Benson et al. 2009 and much of the CLOUD data set (Kirkby et al. 2011; Kürten et al. 2016) except for the 40 % RH at 298 K data. The bulk-source H_2SO_4 data reported by Zollner et al. is included for reference; it was corrected from 38% RH to 52 % RH, increasing by about a factor of 5 using a RH^5 dependency. The difference between the bulk-source and present photolytic H_2SO_4 is about 4 orders of magnitude; the Kürten et al. (2016) 40 % RH data is closest to this set of bulk data, within about two orders of magnitude.

There is apparent agreement of several data sets for H_2SO_4 concentrations of 10^8 to 10^9 cm^{-3}: our lowest J (and the extrapolation of our data, dotted line), Yu et al. (2017), Benson et al. (2009), Kürten et al. (2016) and Kirkby et al. (2012) but it is complicated by the wide range of relative humidities: 2.3 % RH up to 75 % RH. The data of Young et al. (2008) suggests a very low contamination level however there are unresolved issues in measured [H_2SO_4] (see the factor of ten disparity in their Fig. 5). Lack of experimental water dependencies and assessment of base-levels makes drawing conclusions from these comparisons fraught with difficulty. Nonetheless, it is interesting that the dependencies of J on sulfuric acid level are similar in many of these studies. This suggests there is an underlying similarity in particle formation conditions such as contaminant identity and level (which seems unlikely) or the critical cluster's H_2SO_4-content is not particularly sensitive to the type or abundance of the contaminant.

3.4.1 Comparison of nucleation rates for added ammonia

Plotted in Fig. 10 are nucleation rates vs. ammonia abundance for measurements at low [H_2SO_4], $5x10^7$ and $1.5x10^8$ cm^{-3}, and temperatures between 288 and 293 K. Also plotted are predictions according to the present data using the box-model and methodology presented in Hanson et al. (2017). The experimental data from the CLOUD project for 292.5 K were taken from Dunne et al. (2017) and were also presented by Kürten et al. (2016). The Benson et al. (2009, 2011) work was performed at 288 K and significant extrapolation of nucleation rates were applied to get comparable sulfuric acid concentrations (see the caption). The Berndt et al. (2011) work was performed at 293 K and extrapolation was needed to get comparison rates for the $1.5x10^8$ cm^{-3} [H_2SO_4] conditions.

The model predictions using the NH3_52 thermodynamics developed here gives rates that are congruent with the CLOUD data and with Berndt et al. (2011) while NH3_I thermodynamics (calculated only for [H_2SO_4] = $1.5x10^8$ cm^{-3}) gives rates too high by two-to-three orders of magnitude. NH3_I is a set of ammonia-sulfuric acid thermodynamics derived in Hanson et al. (2017) that skirted the lower limit of the Glasoe et al. (2015) ammonia data set. Benson et al. (2009, 2011) is quite disparate and a temperate correction would lessen the discrepancy for the set of data at the low H_2SO_4 but it would worsen it at the higher H_2SO_4.

With the box-model predictions using NH3_52 thermodynamics serving as a bridge, the present ammonia-added data agrees with both the CLOUD data (Kürten et al., 2016; Dunne et al. 2017) and the Berndt et al. (2011) data. Since the box-model rates using NH3_I thermodynamics (Hanson et al. 2017) are much too high, we can conclude that the Glasoe et al. (2015) ammonia data set it was based on does not agree with the present measurements. Recently, Kürten (2019) concluded that the NH3_II (stronger binding than NH3_I) thermodynamics of Hanson et al. (2017) yields nucleation rates much higher than the CLOUD measurements.

4 Summary

We presented a new experimental apparatus for studying particle formation involving photolytically-formed H_2SO_4 vapor and results show the system is reproducible and responds to changes in water, HONO and SO_2 concentrations largely as expected. Modeled particle formation rates could be made congruous with experimental observations by including either dimethylamine at a level of $5x10^{-15}$ mole fraction or NH_3 at a level of ~$2x10^{-10}$ mole fraction. Also, the dependence of N_p on SO_2 level was best explained by a reaction between HO_2 and SO_2 that yields (ultimately) H_2SO_4 and OH with a rate coefficient of $3x10^{-17}$ cm^3/s.

Comparison of the present results to other photolytic H_2SO_4 experiments yields several suppositions. Their divergence from the bulk-source data of Zollner et al. (2012) suggests these experiments are not clean enough and/or they are subject to an unknown reaction or photochemistry. The similarity of the present results to those of Benson et al. (2009), Kirkby et al. (2011), Kürten et al. (2016) and Yu et al. (2017) suggests a common element that affects nucleation beyond what bulk-source H_2SO_4 experiments reveal. The outlier results of Berndt et al. (2010, 2014) and Benson et al. (2011) may suffer from relatively high level of contaminants: Berndt et al. (2014) suggested that a pptv-level of amine could have been present in their experiment. As can be seen in Fig. 9, there is a remarkable agreement of the H_2SO_4 power dependencies for Kirkby et al. (2011), Yu et al. (2017), and the present results. This may be due to a similarly-sized critical cluster across these studies.

Side products from photolytic generation of H_2SO_4 that enhance nucleation were suggested by Berndt et al. (2008), however, Sipilä et al. (2010) found no difference between nucleation rates whether H_2SO_4 was produced photolytically or taken from a bulk source. Yet much of the Sipilä et al. (2010) photolytic nucleation rates are many orders of magnitude too high for the putative binary system (see Fig. 9 comparing the present results, the Zollner et al. (2012) bulk-liquid data, Yu et al. (2017) and results from the CLOUD experiment: Kirkby et al.(2011), Kürten et al. (2016).) With the exception of their bulk 298 K 30% RH results, the Sipilä et al. (2010) data largely overlap the Benson et al. (2011) and Berndt et al. (2014) data and probably also suffer from amine contaminants at the pptv-level.

The total particle number strongly depended on relative humidity with RH^4 and RH^6 power relationships over RH ranges of 15 to 35 % and 40 to 77%, respectively. The CLOUD 298 K results (Kürten et al., 2016) show a power dependency of 4 on RH from 40 to 75 % at 298 K in rough agreement with the present results. Yu et al. (2017) reported a nucleation rate that depended linearly on RH that seems to be out of line with these other data sets.

The weak dependence of N_p on added NH_3 near room temperature, also reflected in a few other studies (Kirkby et al. 2011; Kürten et al. 2016, Benson et al., 2011), is probably due to a contaminant that overwhelms ammonia-induced nucleation, especially at low levels of added ammonia. We surmised that a contaminant in our system is not consistent with dimethylamine but is consistent with a few hundred pptv of ammonia; alternatively, we postulated that 0.5 pptv of methylamine could also be responsible.

The model simulations with NH_3-H_2SO_4 thermodynamic schemes NH3_I and, because it is stronger, NH3_II (Hanson et al. 2017), result in N_p that greatly exceed the present experimental results. With the simulations serving as a bridge between

these two experiments, we conclude that the present experimental data and the Glasoe et al. (2015) NH_3-H_2SO_4 results do not agree. Glasoe et al. (2015) noted that their NH_3-H_2SO_4 nucleation rates were much higher than those of Ball et al. (1999) and Zollner et al. (2012), but with the present results as a backdrop the Glasoe et al. criticisms of those two studies are blunted. In hindsight we postulate an avenue for an amine contamination in the Glasoe et al. (2015) ammonia experiments: several amino-compounds were studied in succession using the same dynamic dilution system. Since ammonia was used between amines, holdover of the amine is possible and even small levels would significantly boost particle numbers, compromising the ammonia-sulfuric acid system measurements. Note that in the present experimental setup, there were two dynamic dilution systems, one dedicated for ammonia and one for dimethylamine.

Additions of dimethylamine resulted in large abundances of particles which limited the range of conditions we were able to study. The number densities are such that a model with proper treatments of coagulation and cluster- cluster collisions is needed to fully interpret the results. Nonetheless, the experimental results are in decent agreement with model simulations using the thermodynamic scheme (DMA_I, Hanson et al., 2017) that best captured the Glasoe et al. (2015) dimethylamine-H_2SO_4 experimental results. We found low RH dependencies when dimethylamine was added, in line with expectations. Note the details of this preliminary finding need further work: (i) RH affects the steady-state sulfuric acid and (ii) coagulation effects need to be properly evaluated.

Atmospheric implications of the present work are of a qualitative nature. The current work suggests that nucleation rates in the NH_3-H_2SO_4 system for a few studies can be seen to converge but more measurements near room temperature are needed to aid the development of ammonia-sulfuric acid thermodynamics (e.g. this work, Hanson et al. 2017; Kürten, 2019). We concluded that the experimental nucleation rates in this system from Glasoe et al. (2015) are discordant. On the other hand, as alluded to in the previous paragraph, the current work is consistent with the Glasoe et al. (2015) dimethylamine-H_2SO_4 results. Also, the much-predicted low RH dependency for dimethylamine-H_2SO_4 nucleation finds experimental corroboration here. Finally, even if the reaction of HO_2 with SO_2 occurs with a rate coefficient of $1x10^{-16}$ cm^3 s^{-1}, it is probably an insignificant source of atmospheric hydroxyl radicals and oxidized sulfur compounds.

In the future, a series of measurements in the dimethylamine-H_2SO_4 system with added dimethylamine at fractional pptv levels and low relative humidities are planned. We also plan to study the relative humidity dependence of ammonia-induced H_2SO_4 nucleation as well as variations of temperature on both amine- and ammonia-addition nucleation. In the long term, the system developed here will be used in particle growth studies where nm-diameter particles prepared in the Glasoe et al. (2015) apparatus are directed through PhoFR along with target organic compounds.

Data availability. All data presented in this manuscript are available by contacting the corresponding author.

Author contribution.

HA and JV built the particle detector and performed preliminary experiments, MA helped design and carry out experiments, SM carried out added-NH_3 experiments and helped with the manuscript, JK helped develop the photochemical

module, and DH developed and ran the simulations, developed and carried out experiments and prepared the manuscript with contributions from all co-authors. The authors declare that they have no conflict of interest.

Acknowledgements.

Thanks to C. Grieves, C. Ward, N. Hoffmann and S. Thao for performing verification experiments that lead to improvements in the deployment of the DEG system and T. Otsego for data analysis. Thanks to T. Kukowski for programming help on the numerical model. Thanks to Y. Melka and N. Clark for their work on the Python program that accumulates and displays particle counter data. We are grateful to Dr. M. Stolzenburg and Prof. P. McMurry for comments on the manuscript and for lending their expertise and guidance during the course of this work.

References

Almeida, J., Schobesberger, S., Kürten, A., Ortega, I. K., Kupiainen-Määttä, O., Praplan, A. P., Adamov, A., Amorim, A., Bianchi, F., Breitenlechner, M., David, A., Dommen, J., Donahue, N. M., Downard, A., Dunne, E. M., Duplissy, J., Ehrhart, S., Flagan, R. C., Franchin, A., Guida, R., Hakala, J., Hansel, A., Heinritzi, M., Henschel, H., Jokinen, T., Junninen, H., Kajos, M., Kangasluoma, J., Keskinen, H., Kupc, A., Kurtén, T., Kvashin, A. N., Laaksonen, A., Lehtipalo, K., Leiminger, M., Leppä, J., Loukonen, V., Makhmutov, V., Mathot, S., McGrath, M. J., Nieminen, T., Olenius, T., Onnela, A., Petäjä, T., Riccobono, F., Riipinen, I., Rissanen, M., Rondo, L., Ruuskanen, T., Santos, F. D., Sarnela, N., Schallhart, S., Schnitzhofer, R., Seinfeld, J. H., Simon, M., Sipilä, M., Stozhkov, Y., Stratmann, F., Tomé, A., Tröstl, J., Tsagkogeorgas, G., Vaattovaara, P., Viisanen, Y., Virtanen, A., Vrtala, A., Wagner, P. E., Weingartner, E., Wex, H., Williamson, C., Wimmer, D., Ye, P., Yli-Juuti, T., Carslaw, K. S., Kulmala, M., Curtius, J., Baltensperger, U., Worsnop, D. R., Vehkamäki, H., and Kirkby, J.: Molecular understanding of sulphuric acid-amine particle nucleation in the atmosphere, Nature, 502, 359–363, https://doi.org/10.1038/nature12663, 2013.

Ball, S. M., D. R. Hanson, F. L. Eisele, and Peter H. McMurry. "Laboratory Studies of Particle Nucleation - Initial Results for H_2SO_4, H_2O, and NH_3 Vapors." *J Geophys Res* 104 (D19): 23, 718, 1999.

Benson, D. R., Erupe, M.E., and S.-H Lee. "Laboratory-measured H_2SO_4, NH_3, H_2O ternary homogeneous nucleation rates: Initial observations" *Geophys. Res. Lett.* 36, L15818, doi:10.1029/2009GL038728, 2009.

Benson, D. R., J. H. Yu, A. Markovich, and S. -H Lee. "Ternary Homogeneous Nucleation of H_2SO_4, NH_3, and H_2O Under Conditions Relevant to the Lower Troposphere." *Atmos Chem Phys* 11 (10): 4755-4766. doi:10.5194/acp-11-4755-2011, 2011.

Berndt, T., F. Stratmann, Brasel, S., J. Heintzenberg, A. Laaksonen, M. Kulmala "SO_2: oxidation products other than H2SO4 as a trigger for new particle formation. Part 1: Laboratory investigations." *Atmos Chem Phys* 8: 6365-6374. doi:10.5194/acp-8-6365-2008, 2008.

Berndt, T., F. Stratmann, M. Sipilä, J. Vanhanen, T. Petaejae, J. Mikkilae, A. Gruener, Spindler, G., Mauldin III, R., Curtius, J., Kulmala, M., and Heintzenberg, J.: "Laboratory Study on New Particle Formation from the Reaction OH + SO_2: Influence of Experimental Conditions, H_2O Vapour, NH_3 and the Amine Tert-Butylamine on the overall Process." *Atmos Chem Phys* 10 (15): 7101-7116. doi:10.5194/acp-10-7101-2010, 2010.

Berndt, T., Sipilä, M., Stratmann, F., Petäjä, T., Vanhanen, J., Mikkilä, J., Patokoski, J., Taipale, R., Mauldin III, R.L., and M. Kulmala, Enhancement of atmospheric H2SO4/H2O nucleation: organic oxidation products versus amines. Atmos Chem Phys, 14, 751-764. doi:10.5194/acp-14-751-2014, 2014.

Burrows, J. P., D. I. Cliff, G. W. Harris, B. A. Thrush, and J. P. T. Wilkinson. "Atmospheric Reactions of the HO_2 Radical Studied By Laser MRS." *Proc Royal Soc of London. Ser A*, 368: 463-481, 1979.

Chen, X., Cen Tao, Li Zhong, Ya Gao, Wei Yao and Shujin Li, Theoretical study on the atmospheric reaction of SO2 with the HO2 and HO2·H2O complex formation HSO4 and H2SO3, Chem. Phys. Lett., 608, 2720276 2014.

Coffman, D. J. and D. A. Hegg. "A Preliminary Study of the Effect of Ammonia on Particle Nucleation in the Marine Boundary Layer." *J. Geophys. Res., [Atmospheres]* 100 (D4): 7147-7160. doi:10.1029/94JD03253, 1995.

Dunne, E. M., Gordon, H., Kürten, A., Almeida, J., Duplissy, J., Williamson, C., Ortega, I. K., Pringle, K. J., Adamov, A., Baltensperger, U., Barmet, P., Benduhn, F., Bianchi, F., Breitenlechner, M., Clarke, A., Curtius, J., Dommen, J., Donahue, N. M., Ehrhart, S., Flagan, R. C., Franchin, A., Guida, R., Hakala, J., Hansel, A., Heinritzi, M., Jokinen, T., Kangasluoma, J., Kirkby, J., Kulmala, M., Kupc, A., Lawler, M. J., Lehtipalo, K., Makhmutov, V., Mann, G., Mathot, S., Merikanto, J., Miettinen, P., Nenes, A., Onnela, A., Rap, A., Reddington, C. L. S., Riccobono, F., Richards, N. A. D., Rissanen, M. P., Rondo, L., Sarnela, N., Schobesberger, S., Sengupta, K., Simon, M., Sipilä, M., Smith, J. N., Stozkhov, Y., Tomé, A., Tröstl, J., Wagner, P. E., Wimmer, D., Winkler, P. M., Worsnop, D. R., and Carslaw, K. S.: Global atmospheric particle formation from CERN CLOUD measurements, Science, 354, 1119-1123, 2016.

Eisele F. L. and D. J. Tanner, Measurement of the Gas Phase Concentration of H_2SO_4 and Methane Sulfonic Acid and estimates of H_2SO_4 Production and Loss in the Atmosphere, J. Geophys. Res. D, 98, 9001-9010, 1993.

Ehrhart, S., Ickes, L., Almeida, J., Amorim, A., Barmet, P., Bianchi, F., Dommen, J., Dunne, E. M., Duplissy, J., Franchin, A., Kangasluoma, J., Kirkby, J., Kürten, A., Kupc, A., Lehtipalo, K., Nieminen, T., Riccobono, F., Rondo, L., Schobesberger, S., Steiner, G., Tomé, A., Wimmer, D., Baltensperger, U., Wagner, P. E., and Curtius, J.: Comparison of the SAWNUC model with CLOUD measurements of sulphuric acid water nucleation, J. Geophys. Res.-Atmos., 121, 12401–12414, https://doi.org/10.1002/2015JD023723, 2016.

Febo, A., Perrino, C., Sparapani, R. and Gherardi, M.: Evaluation of a High-Purity and High-Stability Continuous Generation System for Nitrous Acid, Environ. Sci. Tech., 29, 2390-2395, 1995.

Friese, E. and Ebel, A., Temperature Dependent Thermodynamic Model of the System $H^+-NH_4^+-Na^+-SO_4^{2-}-NO_3^--Cl^--H_2O$, J. Phys. Chem. A, 114, 11595-11631, 10.1021/jp101041j, 2010.

Freshour, N., K. K. Carlson, Y. A. Melka, S. Hinz, B. Panta, and D. R. Hanson "Quantifying Amine Permeation Sources with Acid Neutralization: Calibrations and Amines Measured in Coastal and Continental Atmospheres." *Atmos. Meas. Tech.* 7: 3835-3861, 2014.

Glasoe, W. A., K. Volz, B. Panta, N. Freshour, R. Bachman, D. R. Hanson, P. H. McMurry, and C. N. Jen. "Sulfuric Acid Nucleation: An Experimental Study of the Effect of Seven Bases." *J. Geophys. Res. D.* 120, 2015.

Graham, R.A., A M Winer, R Atkinson, and J Pitts Jr. "Rate Constants for the Reaction of HO_2 with HO_2, SO_2, CO, N_20, Trans-2-Butene, and 2,3-Dimethyl-2-Butene at 300 K." *J. Phys. Chem.* 83, 1979.

Hanson, D. R., I. Bier, B. Panta, C. N. Jen, and P. H. McMurry. "Computational Fluid Dynamics Studies of a Flow Reactor: Free Energies of Clusters of Sulfuric Acid with NH_3 and Dimethylamine." *J. Phys. Chem. A* 121 (20): 3976, 2017.

Henschel, H., T. Kurten, and H. Vehkamaki "Computational Study on the Effect of Hydration on New Particle Formation in the Sulfuric Acid/Ammonia and Sulfuric Acid/Dimethylamine Systems," *J. Phys. Chem. A* 120, 1886-1896. doi:10.1021/acs.jpca.5b11366, 2016.

Intergovernmental Panel on Climate Change (2013), Climate Change 2013: IPCC 5th Assessment Report (AR5), Edited, 2013.

Jiang, J., M. Chen, C. Kuang, M. Attoui, and P. H. McMurry. "Electrical Mobility Spectrometer using a Diethylene Glycol Condensation Particle Counter for Measurement of Aerosol Size Distributions Down to 1 Nm." *Aerosol Science and Technology* 45 (4): 510-521. doi:10.1080/02786826.2010.547538, 2011.

Kirkby, J., Curtius, J., Almeida, J., Dunne, E., Duplissy, J., Ehrhart, S., Franchin, A., Gagné, S., Ickes, L., Kürten, A., Kupc, A., Metzger, A., Riccobono, F., Rondo, L., Schobesberger, S., Tsagkogeorgas, G., Wimmer, D., Amorim, A., Bianchi, F., Breitenlechner, M., David, A., Dommen, J., Downard, A., Ehn, M., Flagan, R.C., Haider, S., Hansel, A., Hauser, D., Jud, W., Junninen, H., Kreissl, F., Kvashin, A., Laaksonen, A., Lehtipalo, K., Lima, J., Lovejoy, E. R., Makhmutov, V., Mathot, S., Mikkilä, J., Minginette, P., Mogo, S., Nieminen, T., Onnela, A., Pereira, P., Petäjä, T., Schnitzhofer, R., Seinfeld, J. H., Sipilä, M., Stozhkov, Y., Stratmann, F., Tomé, A., Vanhanen, J., Viisanen, Y., Vrtala, A., Wagner, P. E., Walther, H., Weingartner, E., Wex, H., Winkler, P. M., Carslaw, K. S., Worsnop, D. R., Baltensperger, U., and Kulmala, M.: Role of sulphuric acid, ammonia and galactic cosmic rays in atmospheric aerosol nucleation, Nature, 476, 429–435, https://doi.org/10.1038/nature10343, 2011..

Kreyling, W. G., Semmler-Behnke, M. and Moller, W.: Ultrafine Particle-Lung Interactions: Does Size Matter? J. Aerosol Medicine, 19, 74-83, 10.1089/jam.2006.19.74, 2006.

Kuang, C., M. Chen, J. Zhao, J. Smith, P. H. McMurry, and J. Wang. "Size and Time-Resolved Growth Rate Measurements of 1 to 5 Nm Freshly Formed Atmospheric Nuclei." *Atmospheric Chemistry and Physics* 12 (7): 3573-3589. doi:10.5194/acp-12-3573-2012, 2012.

Kulmala, M., H. Vehkamaki, T. Petaja, M. Dal Maso, A. Lauri, V. -M Kerminen, W. Birmili, and P. H. McMurry. "Formation and Growth Rates of Ultrafine Atmospheric Particles: A Review of Observations." *Journal of Aerosol Science* 35 (2): 143-176. doi:10.1016/j.jaerosci.2003.10.003, 2004.

Kürten, A., L. Rondo, S. Ehrhart, and J. Curtius, “Calibration of a Chemical Ionization Mass Spectrometer for the Measurement of Gaseous Sulfuric Acid” J. Phys. Chem. A, 2012, 116, 6375−6386, dx.doi.org/10.1021/jp212123n.

Kürten, A., C. Williamson, J. Almeida, J. Kirkby, and J. Curtius. "On the Derivation of Particle Nucleation Rates from Experimental Formation Rates." *Atmospheric Chemistry and Physics* 15 (8): 4063-4075. doi:10.5194/acp-15-4063-2015, 2015.

Kürten, A., Bianchi, F., Almeida, J., Kupiainen-Määttä, O., Dunne, E. M., Duplissy, J., Williamson, C., Barmet, P., Breitenlechner, M., Dommen, J., Donahue, N. M., Flagan, R. C., Franchin, A., Gordon, H., Hakala, J., Hansel, A., Heinritzi, M., Ickes, L., Jokinen, T., Kangasluoma, J., Kim, J., Kirkby, J., Kupc, A., Lehtipalo, K., Leiminger, M., Makhmutov, V., Onnela, A., Ortega, I. K., Petäjä, T., Praplan, A. P., Riccobono, F., Rissanen, M. P., Rondo, L., Schnitzhofer, R., Schobesberger, S., Smith, J. N., Steiner, G., Stozhkov, Y., Tomé, A., Tröstl, J., Tsagkogeorgas, G., Wagner, P. E., Wimmer, D., Ye, P., Baltensperger, U., Carslaw, K., Kulmala, M., and Curtius, J.: Experimental particle formation rates spanning tropospheric sulfuric acid and ammonia abundances, ion production rates and temperatures, J. Geophys. Res.-Atmos., 121, 12377–12400, https://doi.org/10.1002/2015JD023908, 2016.

Kürten, A., Li, C., Bianchi, F., Curtius, J., Dias, A., Donahue, N. M., Duplissy, J., Flagan, R. C., Hakala, J., Jokinen, T., Kirkby, J., Kulmala, M., Laaksonen, A., Lehtipalo, K., Makhmutov, V., Onnela, A., Rissanen, M. P., Simon, M., Sipilä, M., Stozhkov, Y., Tröstl, J., Ye, P., and McMurry, P. H.: New particle formation in the sulfuric acid-dimethylamine-water system: reevaluation of CLOUD chamber measurements and comparison to an aerosol nucleation and growth model, Atmos. Chem. Phys., 18, 845–863, https://doi.org/10.5194/acp-18-845-2018, 2018.

Kürten, A. New particle formation from sulfuric acid and ammonia: nucleation and growth model based on thermodynamics derived from CLOUD measurements for a wide range of conditions, Atmos. Chem. Phys., 19, 5033–5050, 2019. https://doi.org/10.5194/acp-19-5033-2019

Kurten, T., V. Loukonen, H. Vehkamaki, and M. Kulmala. "Amines are Likely to Enhance Neutral and Ion-Induced Sulfuric Acid-Water Nucleation in the Atmosphere More Effectively than Ammonia." *Atmospheric Chemistry and Physics* 8 (14): 4095-4103. doi:10.5194/acp-8-4095-2008, 2008.

Kurten, T., J. R. Lane, S. Jørgensen, and H. G. Kjaergaard, A Computational Study of the Oxidation of SO2 to SO3 by Gas-Phase Organic Oxidants, J. Phys. Chem. A, 115, 8669–8681, 2011. dx.doi.org/10.1021/jp203907d

Larriba, A., Hogan, C. and de Lamora, J.: The Mobility–Volume Relationship below 3.0 nm Examined by Tandem Mobility–Mass Measurement, Aerosol Science and Technology, 45, 453-467, 2010.

Lovejoy, E. R., Hanson, D. R. and Huey, L. G.: Kinetics and Products of the Gas-Phase Reaction of SO_3 with Water, J. Phys. Chem., 100, 19911-19916, 1996.

McMurry, P. H. "New Particle Formation in the Presence of an Aerosol: Rates, Time Scales, and Sub-0.01 Um Size Distributions," *Journal of Colloid and Interface Science* 95 (1): 72-80. doi:10.1016/0021-9797(83)90073-5, 1983.

McMurry, P. H., M. Fink, H. Sakurai, M. R. Stolzenburg, R. L. Mauldin III, J. Smith, F. Eisele, et al. "A Criterion for New Particle Formation in the Sulfur-Rich Atlanta Atmosphere." *J. Geophys. Res.,* 110 (D22): D22S02/10. doi:10.1029/2005JD005901, 2005.

Nadykto, A. and F. Yu. "Amine's in the Earth's Atmosphere: A Density Functional Theory Study of the Thermochemistry of Pre-Nucleation Clusters," *Entropy* 13: 554-569, 2011.

Nel, A. "Air Pollution-Related Illness: Effects of Particles." *Science* 308 (5723): 804-806. doi:10.1126/science.1108752, 2005.

Ortega, I. K., O. Kupiainen, T. Kurten, T. Olenius, O. Wilkman, M. J. McGrath, V. Loukonen, and H. Vehkamaki. "From Quantum Chemical Formation Free Energies to Evaporation Rates." *Atmospheric Chemistry and Physics* 12 (1): 225-235. doi:10.5194/acp-12-225-2012, 2012.

Panta, B, W A Glasoe, J H Zollner, K K. Carlson, and D. R. Hanson "Computational Fluid Dynamics of a Cylindrical Nucleation Flow Reactor with Detailed Cluster Thermodynamics," *J. Phys. Chem. A* 116: 10122-10134. doi:10.1021/jp302444y, 2012.

Payne, W. A., L. J. Stief, and D. D. Davis. "A Kinetics Study of the Reaction of HO_2 with SO_2 and NO;" *J. Am. Chem. Soc.* 95: 7614-7619, 1973.

Sipilä, M., Berndt, T., Petaejae, T., Brus, D., Vanhanen, J. Stratmann, F., Patokoski, J., Mauldin, L., Hyvärinen, A.-P., Lihavainen, H., and Kulmala, M.: "The Role of Sulfuric Acid in Atmospheric Nucleation." *Science* 327: 1243-1246. doi:10.1126/science.1180315, 2010.

Sörgel, M., E. Regelin, H. Bozem, J. -M Diesch, F. Drewnick, H. Fischer, H. Harder, et al. "Quantification of the Unknown HONO Daytime Source and its Relation to NO_2." *Atmos Chem Phys* 11(20): 10433-10447. doi:10.5194/acp-11-10433-2011, 2011.

Viisanen, Y., M Kulmala, and A Laaksonen. "Experiments on Gas-Liquid Nucleation of Sulfuric Acid and Water." *Journal of Chemical Physics* 107 (3): 920-926. doi:10.1063/1.474445, 1997.

Verheggen, B. and M. Mozurkewich. "Determination of Nucleation and Growth Rates from Observation of a SO_2 Induced Atmospheric Nucleation Event." *J Geophys Res* 107, doi:10.1029/2001JD000683, 2002.

Wexler, A. S. and S. L. Clegg. "Atmospheric Aerosol Models for Systems Including the Ions H+, NH_4+, Na+, SO_4^{2-}, NO_3^-, Cl^-, Br^-, and H_2O." *J Geophys Res* 107 (D14): 4207. doi:10.1029/2001JD000451, 2002.

Wyslouzil, B. E., J. H. Seinfeld, R. C. Flagan, and K. Okuyama. "Binary Nucleation in Acid-Water Systems. II. Sulfuric Acid-Water and a Comparison with Methanesulfonic Acid-Water." *Journal of Chemical Physics* 94 (10): 6842-6850. doi:10.1063/1.460262, 1991.

Young, L. H., Benson, D. R., Kameel, F. R., Pierce, J. R., Junninen, H., Kulmala, M., and Lee, S.-H.: Laboratory studies of H_2SO_4/H_2O binary homogeneous nucleation from the SO_2+OH reaction: evaluation of the experimental setup and preliminary results, Atmos. Chem. Phys., 8, 4997–5016, doi:10.5194/acp-8-4997-2008, 2008.

Yu, H., L Dai, Y Zhao, V P. Kanawade, S N. Tripathi, X Ge, M Chen, and S.-Hu Lee. "Laboratory Observations of Temperature and Humidity Dependencies of Nucleation and Growth Rates of Sub-3 nm Particles." *J. Geophys. Res.: Atmospheres* 122 (3): 1919-1929. doi:10.1002/2016JD025619, 2017.

Yu, H, R McGraw, and S-H Lee. "Effects of Amines on Formation of Sub-3 Nm Particles and their Subsequent Growth." *Geophysical Research Letters* 39. doi:10.1029/2011GL050099, 2012.

Zollner, J. H., W. A. Glasoe, B. Panta, K. K. Carlson, P. H. McMurry, and D. R. Hanson. "Sulfuric Acid Nucleation: Power Dependencies, Variation with Relative Humidity, and Effect of Bases," *Atmospheric Chemistry and Physics* 12 (10): 4399-4411. doi:10.5194/acp-12-4399-2012, 2012.

Figures and captions.

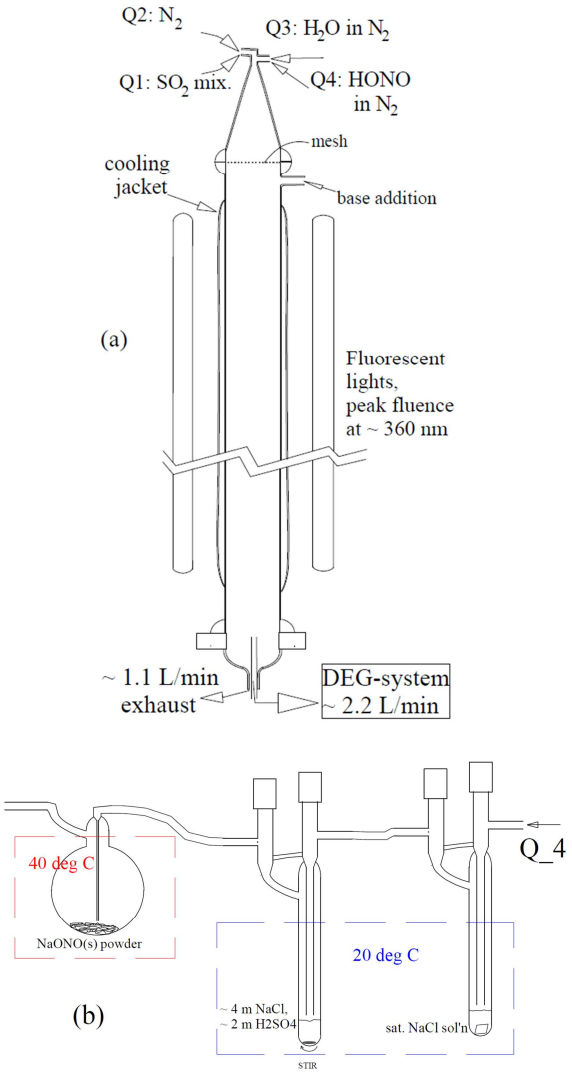

Fig. 1 (a) PhoFR schematic and (b) HONO source. The average flow velocity of 2.8 cm/s yields an average residence time in PhoFR of approximately 45 s. The concentrations listed in (b) are in molal (mole per kg H_2O).

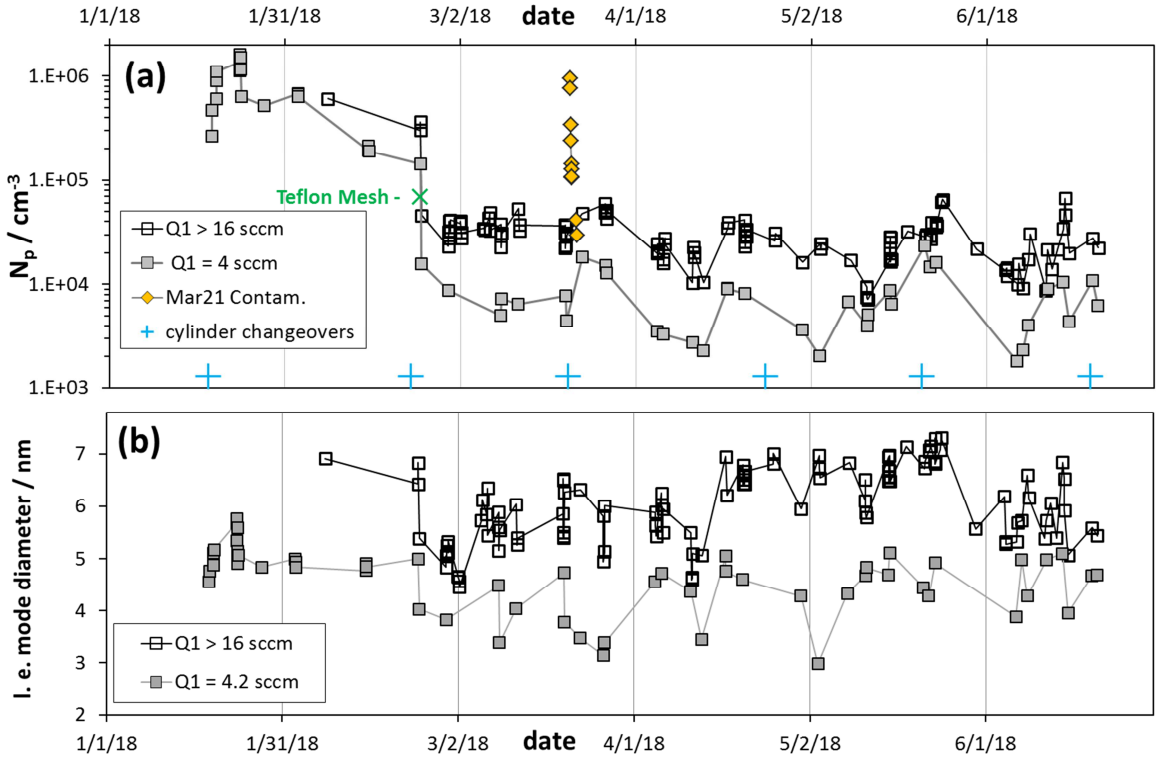

Fig. 2. (a) Number of large particles for baseline HONO (Q_4=4.2 sccm: [HONO] = 5x10^{11} cm^{-3}) plotted vs. time for two different SO_2 levels, equivalent to 2 and > 8 ppmv. Data on 21 and 22 Mar are shown as the yellow diamonds and are for low SO_2 conditions: N_p is severely elevated due to a suspected dust contaminant. (b) Leading edge mode diameters plotted versus time also binned by SO_2 level.

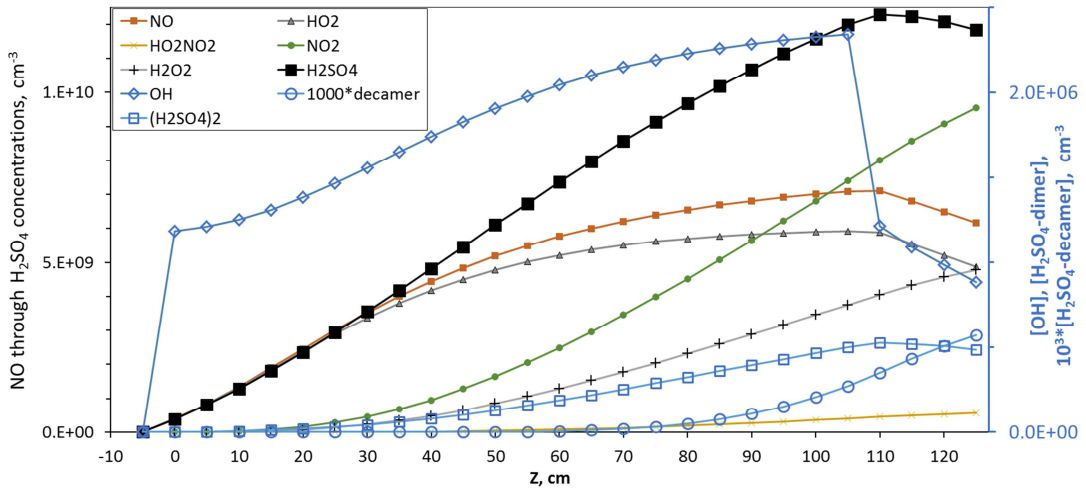

Fig. 3. Model simulation for [HONO]= 5.2x10^{11} cm^{-3}, [SO_2] = 4x10^{14} cm^{-3} and no base. Concentrations of NO through H_2SO_4 are plotted on the left axis; concentrations of OH and the $(H_2SO_4)_2$ and $(H_2SO_4)_{10}$ clusters on the right axis. These simulations are equivalent to experimental conditions of Q_4=4.2 sccm, Q_1 = 32 sccm. The lighted section is from 0 to 110 cm. At 110 cm HONO photolysis ceases and [OH] (right axis) drops to a level supplied by HO_2 + NO.

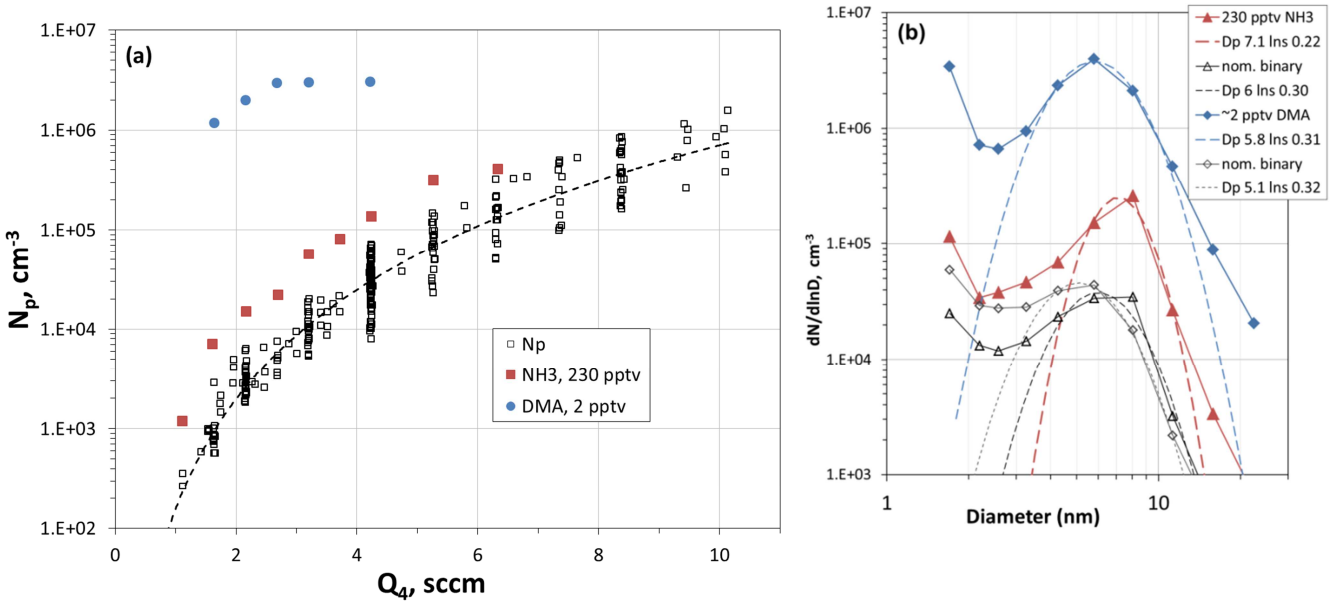

Fig. 4. (a) Number of large particles as a function of Q_4, the HONO-laden flow rate. RH was 52 %, T = 296 K, and $[SO_2] > 2.5x10^{14}$ cm^{-3}. For reference, Q_4 = 4.2 sccm results in a modeled value of ~ $4x10^9$ cm^{-3} for H_2SO_4 at Z = 35 cm and R = 0. Base-added experimental results are shown as the circles (dimethylamine) and red squares (ammonia). (b) Size distributions showing the effect of added NH_3 (red triangles) and added dimethylamine (blue diamonds). Nominal binary distributions for those runs are also shown. The log-normal distributions are also shown (dashed lines) and the legend indicates the mode diameter and lnσ in that order.

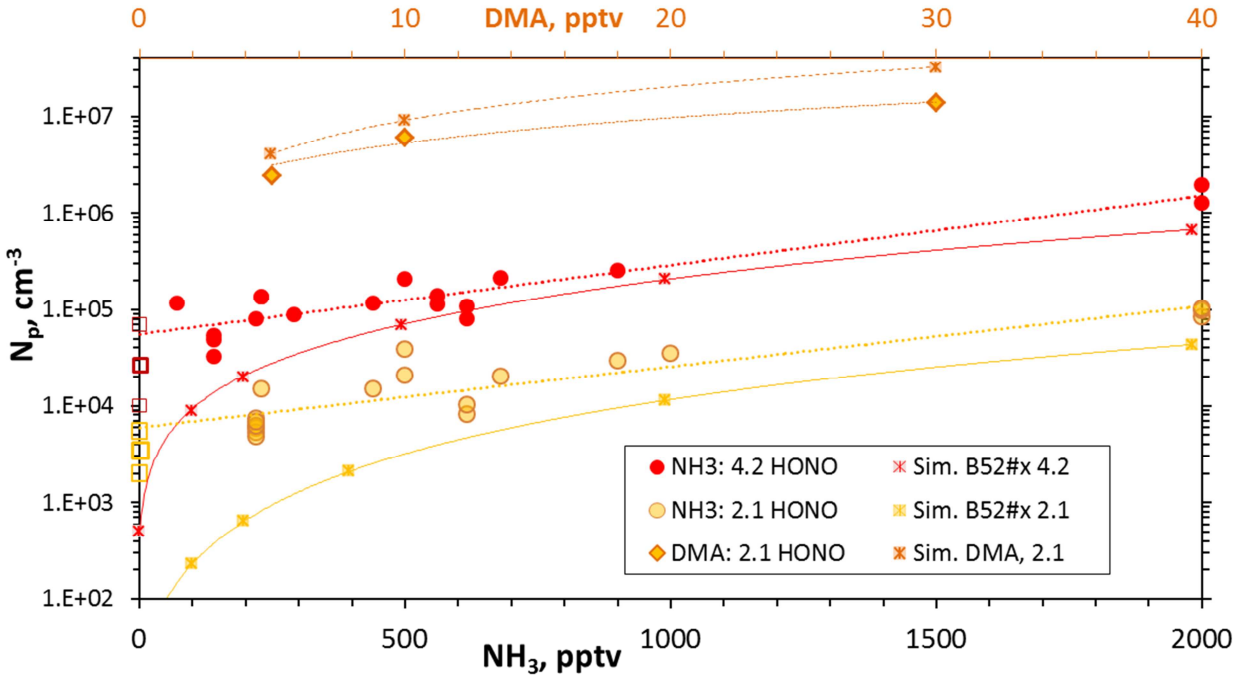

Fig. 5. Variation of measured N_p with added NH_3 for Q_4 of 4.2 sccm and 2.1 sccm and for added dimethylamine at Q_4 = 2.1 sccm (top axis for dimethylamine level). Simulated N_p are shown for NH3_52 (ammonia) and DMA_I (dimethylamine) thermodynamics. The average and the range of measured N_p without added base are shown as the squares for the two Q_4 levels.

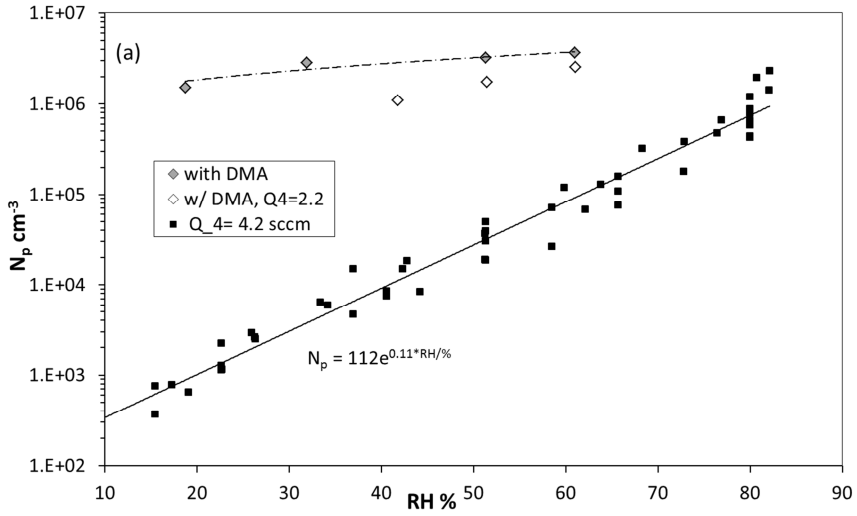

Fig. 6. Variation of $N_p$with RH in % (RH determined by the fraction of flow through the water saturator, Q_3) Q_4 was 4.2 sccm and Q_1 > 20 sccm. Also shown are data with dimethyl amine added: at 2 pptv (filled diamonds) and data at a lower Q_4 = 2.1 sccm and dimethyl amine at 5 pptv.

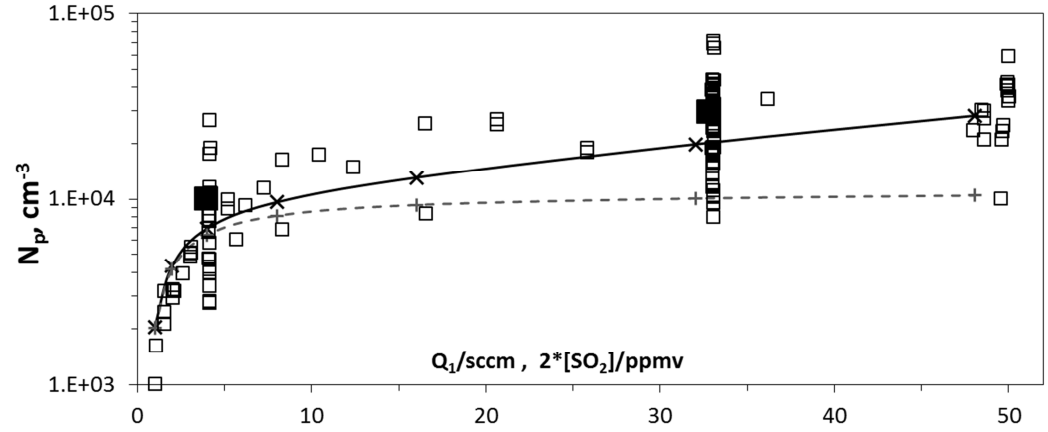

Fig. 7. Number of large particles vs. flow rate of SO_2 mixture. The HONO-source flow rate, Q_4, was 4.2 sccm which results in roughly 5x10^{11} cm^{-3} [HONO] in PhoFR. For reference, an SO_2 mixture flow rate of 32 sccm results in an [SO_2] of 4x10^{14} cm^{-3} in PhoFR (about 16 pptv). The solid and dashed lines are model values for N_p and size with 200 pptv NH_3 entering the flow reactor and a k3x5 (HO_2 + SO_2) rate coefficient of 3x10^{-17} cm^3/s (x's, solid lines) and in the absence of this reaction (+'s and dashed lines). The solid squares indicate the average at Q_1 = 4 and 32 sccm.

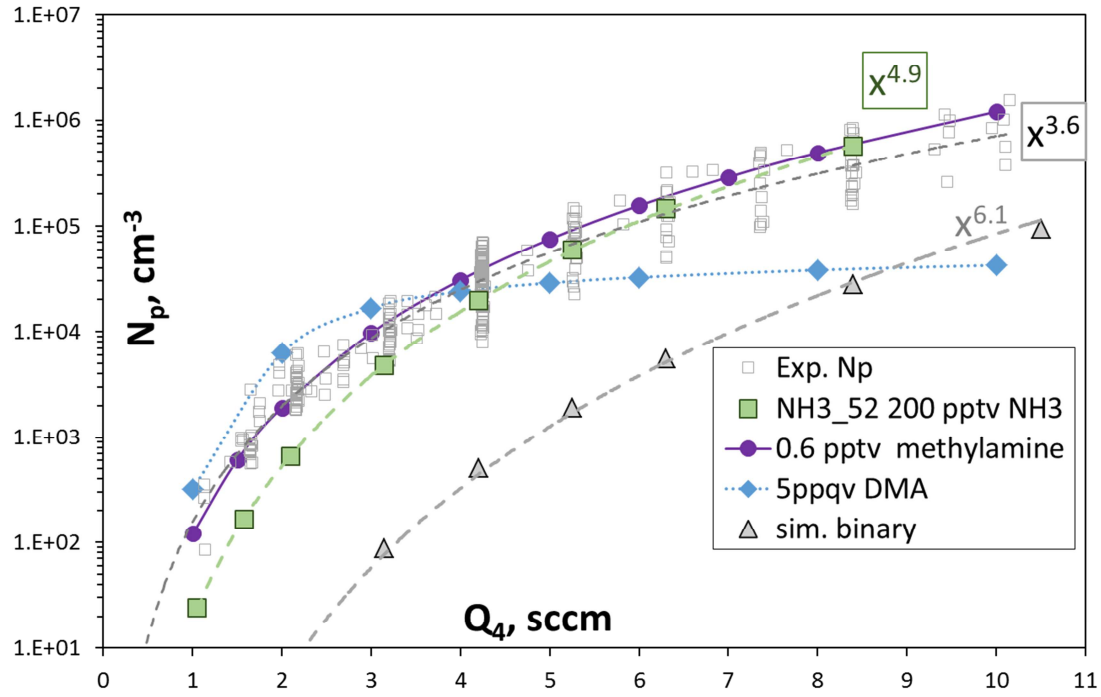

Figure 8. Np vs. Q_4, the HONO-containing flow. Experimental from Fig. 4(a), simulated is on-axis Np at axial position = 120 cm into PhoFR. Green symbols are ammonia at 200 pptv and the gray triangles are the binary, simulated with scheme NH3_52 thermodynamics; the blue diamonds are simulations with 0.005 pptv dimethylamine added using DMA_I thermodynamics. The purple circles are 0.6 pptv methylamine from Glasoe et al. (2015). Power dependencies indicated in the plot.

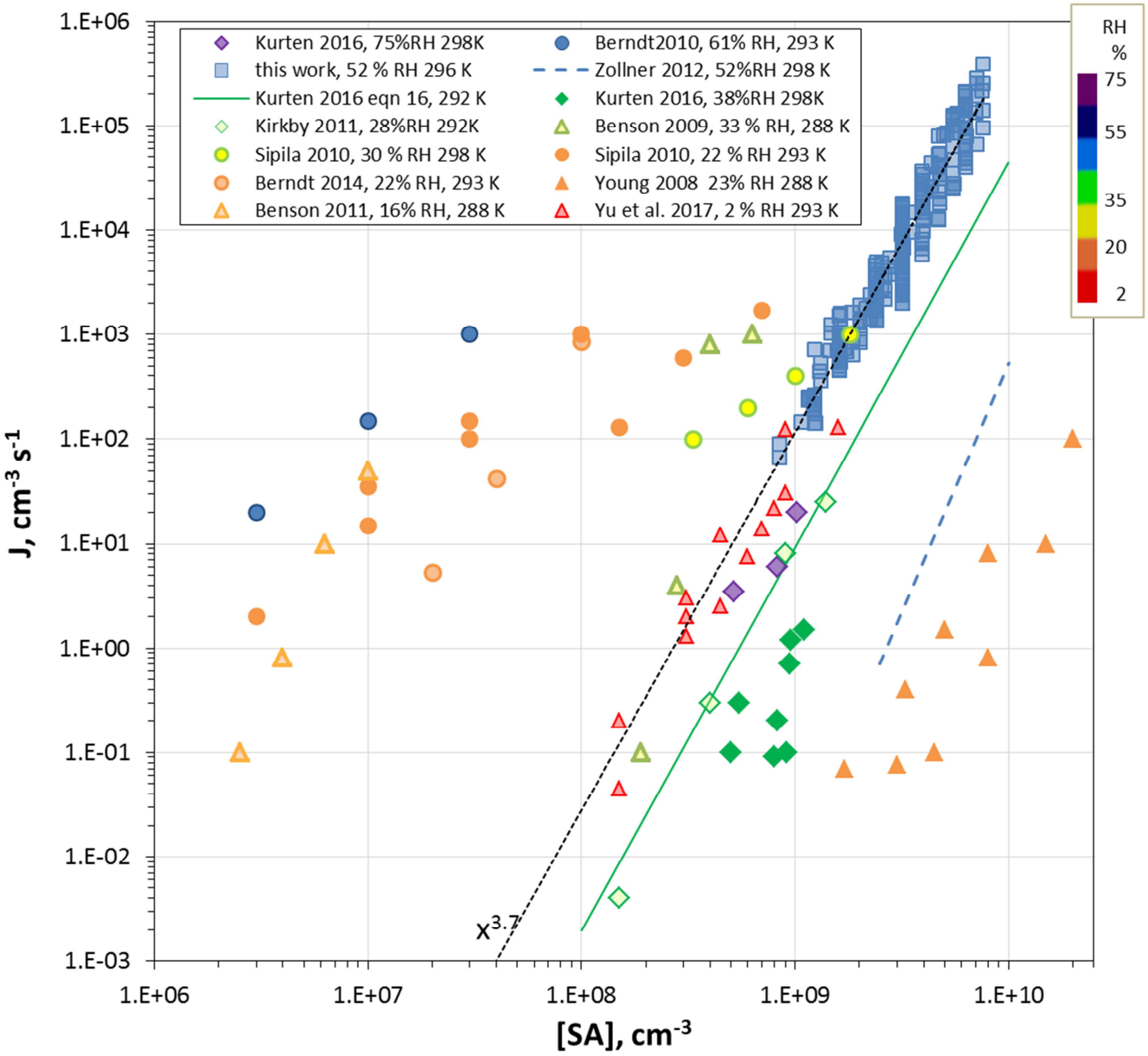

Fig. 9: Comparison of results from previous work (all photolytic H_2SO_4 production except Zollner et al., 2012) for nominally clean conditions. RH color-coding was applied to the points and temperatures are indicated in the legend.

5

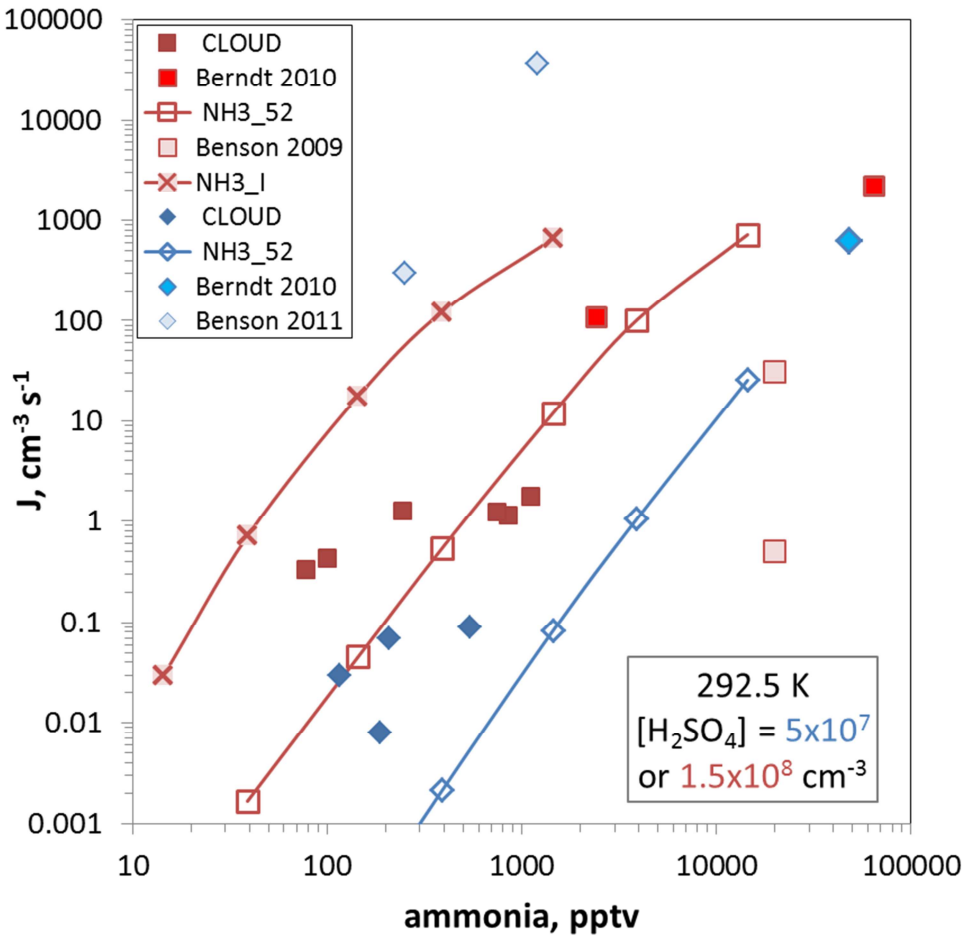

Fig. 10. Ammonia-sulfuric acid nucleation rate vs. ammonia abundance. Sulfuric acid level is $5x10^7$ cm^{-3} for the blue diamonds and $1.5x10^8$ cm^{-3} for the red squares. CLOUD data is from Dunne et al., 292.5 K, neutral conditions. Berndt et al. (2010), 293 K, has their squared dependence on $[H_2SO_4]$ applied which results in a division by ~30 to extrapolate to the $1.5x10^8$ cm^{-3} conditions; no corrections needed for the $5x10^7$ cm^{-3} data point. Benson et al. (2009) report a 4 power dependence on sulfuric acid and correction factors are 5 and divide by 16. Benson et al. (2011) requires multiplicative factors of ~40 to extrapolate to $5x10^7$ cm^{-3} $[H_2SO_4]$. Box model nucleation rates for the two different $[H_2SO_4]$ are shown for the NH3_52 thermodynamics and J for the $1.5x10^8$ cm^{-3} conditions was also predicted using NH3_I from Hanson et al. (2017).